

# Optimum Design of an 18-Pulse Phase Shifting Autotransformer Rectifier to Improve the Power Quality of Cascaded H-Bridge Motor Driver

Adil Alahmad\*, Firat Kacar, Cengiz Polat Uzunoglu

Department of Electrical and Electronics Engineering, Istanbul University - Cerrahpasa,  
Baglarici Cd. No: 7, 34320 Avcilar, Istanbul, Turkey

\*adil.alahmad@hotmail.com; fkacar@iuc.edu.tr; polat@iuc.edu.tr

**Abstract**—Due to its simplicity, efficiency, and dependability, the multipulse rectifier is widely used in electrical systems. In the presented work, an optimum design of an 18-pulse rectifier is achieved by comparing the most used configurations on the market. The 18-phase shifting autotransformer (18-PSAT) rectifier is a cheaper alternative to conventional rectifiers to reduce system harmonics. After a thorough study of the market needs and available use, this paper discusses four different structures that provide harmonic levels according to IEEE 519 limitations. An innovative 18-PSAT is shown, studied, simulated, produced, and tested with low power loss rates. The Delta differential configuration primarily emphasises lowering the loss power rating for improved power quality. With its simple structure, easy assembly, and direct connection to diodes, the proposed Delta differential configuration provides higher power quality and can cancel harmonics. To determine which 18-PSAT rectifier unit has the best weight, size, and power quality, a comparison of the selected topologies is made. A comprehensive comparison of each topology has simulation results showing current, voltage, and total harmonic distortion (THD) using MATLAB Simulink. The simulation results show that the total harmonic distortion is under 2.9 % when adopting the suggested Delta differential configuration topology. Compared to other designs, the suggested 18-pulse layout reduces overall cost and footprint by a large margin. It is also demonstrated that the DC load power is about 85 % of the recommended rectifier rating.

**Index Terms**—Total harmonic distortion (THD); Topology; Multiwinding transformers; 18-pulse rectifiers; 18-phase shifting autotransformer (PSAT); Phase shifting transformer.

## I. INTRODUCTION

In the last 20 years, several multi-pulse rectifier structures have been developed to improve power quality in various industrial implementations, including smart grid systems, aircraft systems, movement and propulsion systems, electrical aviation systems, and high-voltage DC transmission lines [1]. The 18-phase shifting autotransformer (18-PSAT) rectifiers have low harmonic distortion, lower harmonic content, high efficiency, easy to assemble, resilience, and good power factor correction [2]. At the same time, 18-PSAT designs must meet or exceed the standards requirement [3]. One of the primary ways to improve the parameters of power quality is to increase the number of output pulses in PSATs,

which will increase the cost due to components, design complexity, and increased weight and size [4]. The high total harmonic distortion (THD) of 18-PSAT rectifiers cannot meet the IEC standard requirements [5], [6]. Various research suggests the use of phase shifting transformers with unique designs, auxiliary circuits, and active or passive filters on one or both sides of rectifiers to solve THD problems [7], [8]. The 18-PSAT is connected to the converter through a 6-pulse bridge rectifier [9], [10]. In [11], the authors propose a 20-PSAT rectifier that reduces THD by less than 8 %. In [12], a low-rating autotransformer is proposed that reduces the complexity of the design and the total cost. Secondary winding is associated with an active rectifier, which has a potential increase in complexity, losses, and overall manufacturing costs [13], [14]. Magnetic component ratings may be decreased when using designs based on autotransformers, as the magnetic components used are a fraction of the power rate [15]. The 18-PSAT cancels the 5<sup>th</sup>, 7<sup>th</sup>, 11<sup>th</sup>, 13<sup>th</sup>, 23<sup>rd</sup>, 25<sup>th</sup>, 29<sup>th</sup>, and 31<sup>st</sup> harmonics, but it cannot cancel the 17<sup>th</sup>, 19<sup>th</sup>, 35<sup>th</sup>, and 37<sup>th</sup> harmonics and thus cannot cover the IEEE 519 requirement [16].

## II. PROPOSAL CONFIGURATIONS OF 18-PSAT

The purpose of the current work is to find simplicity, efficiency, and dependability from the most widely used 18-PSAT configurations and topologies on the market to achieve the desired outcomes. The 18-PSAT functioning calls for three groups of three-phase alternating current sources, one in phase with the primary voltage and the other displaced by determined angles [17]. An autotransformer system was developed to meet the need for a compact, lightweight, and inexpensive alternative [18]. This article compares autotransformer topologies that do not need additional parts, such as zero sequence blocking transformers (ZSBT) or interphase transformers (IPT), to maximise space and weight savings while maintaining efficiency [19]. The four topologies of 18-PSAT are described.

### A. Symmetric 18-PSAT Fork Differential

The fork configuration reduces the input voltage by 88 %, divides it into three identical sets (each set is three phase), and between each set 40 degrees. As a result, the DC voltage at output equals only 0.41 of line voltage, which is only 4.2 %

more than a standard design. Figure 1(a) shows the connection diagram of the input terminal (power supply) and

the output side (diode bridge). Figure 1(b) shows the conduction sequence.

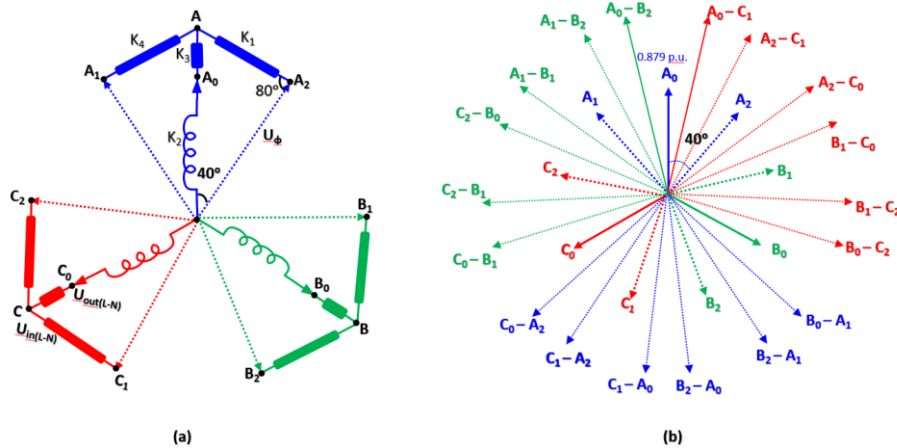


Fig. 1. Symmetric fork: (a) Connection diagram; (b) Conducting sequence.

Assume, in symmetric 18-PSAT fork differential,  $U_{in(LL)}$  refers to the input line voltage,  $U_{in(LN)}$  is the input phase voltage,  $U_{out(LL)}$  refers to the output line voltage,  $U_{out(LN)}$  is the output phase voltage,  $K_1$  is the winding ratio,  $U_{K1}$  is the voltage on the  $K_1$  winding, and  $U_{K2}$  voltage on the  $K_2$  winding.  $U_{K1}$  is calculated as in (1) [19]

$$\frac{U_{K_1}}{\sin 40^\circ} = \frac{U_{in(LN)}}{\sin 80^\circ} \rightarrow U_{K_1} = 0.65 U_{in(LN)}. \quad (1)$$

The  $U_{K_2}$  and  $U_{K_3}$  are determined by (2) and (3):

$$U_{K_2} = U_{out(LN)} = 0.88 U_{in(LN)}, \quad (2)$$

$$U_{K_3} = 0.12 U_{in(LN)}. \quad (3)$$

The  $U_{dc}$  is the DC output voltage and could be calculated

by (4) and (5) [20]:

$$U_{dc} = 0.98 U_{out(LL)}, \quad (4)$$

$$U_{dc} = 0.98 \times 1.73 \times 0.88 U_{in(LN)} = 1.69 U_{in(LN)}. \quad (5)$$

Assuming  $K_1 = 0.35$ ,  $K_2 = 0.48$ ,  $K_3 = 0.15$ ,  $I_{k1} = 0.26 I_{dc}$ ,  $I_{k2} = 0.23 I_{dc}$ , and  $I_{k3} = 0.18 I_{dc}$ , and using Kirchhoff's current law (the total number of ampere turns at nodes A, B, and C equals zero), it allows writing the expressions of the  $I_{in}$  input current using (6) and (7) [18]:

$$I_{in} = I_{K_1} + I_{K_2} + I_{K_3} = 0.26 I_{dc} + 0.23 I_{dc} + 0.18 I_{dc}, \quad (6)$$

$$I_{in} = 0.67 I_{dc}. \quad (7)$$

The MATLAB simulation of the symmetric 18-PSAT fork differential is shown in Fig. 2 using assumed parameters.

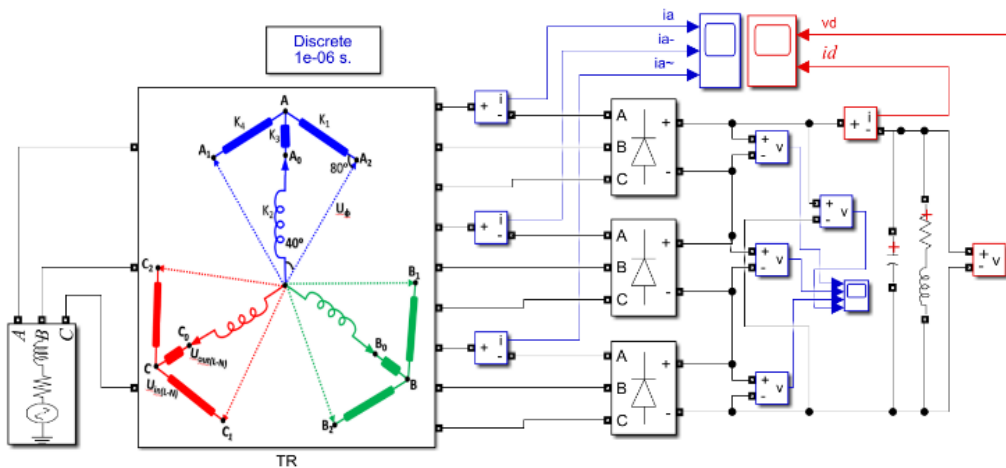


Fig. 2. MATLAB simulation of symmetric fork differential.

The power capacity of an autotransformer can be determined by (8)–(13):

$$C_T = 6K_1 U_{K_1} I_{K_1} + 3K_2 U_{K_2} I_{K_2} + 3K_3 U_{K_3} I_{K_3}, \quad (8)$$

$$6K_1 U_{K_1} I_{K_1} = 6 \times 0.35 \times 0.65 U_{dc} \times 0.26 I_{dc}, \quad (9)$$

$$3K_2 U_{K_2} I_{K_2} = 3 \times 0.48 \times 0.88 U_{dc} \times 0.23 I_{dc}, \quad (10)$$

$$3K_3 U_{K_3} I_{K_3} = 3 \times 0.15 \times 0.12 U_{dc} \times 0.18 I_{dc}, \quad (11)$$

$$C_T = 0.35 U_{dc} I_{dc} + 0.27 U_{dc} I_{dc} + 0.009 U_{dc} I_{dc}, \quad (12)$$

$$\text{Total power capacity} = 0.63 U_{dc} I_{dc}. \quad (13)$$

The total power capacity of the symmetric 18-PSAT fork differential autotransformer equals to 63 % of the load power.

### B. Symmetric 18-PSAT T-Delta Differential

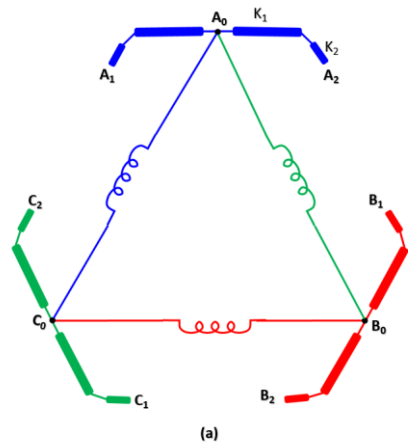
The T-Delta differential configuration divides the input voltage into three identical sets (each set is three phase), and between each set 40 degrees. Figure 3(a) shows the connection diagram of the input terminal (power supply) and the output side (diode bridge). By sharing current with the other two diodes at a rate of 20 % each, each diode can carry 40 % of the total current. The conducting sequence of the diode current in the symmetric 18-PSAT T-Delta differential is shown in Fig. 3(b).

In the symmetric 18-PSAT T-Delta differential, the  $U_{out(LN)}$  is calculated as in (14) [20]

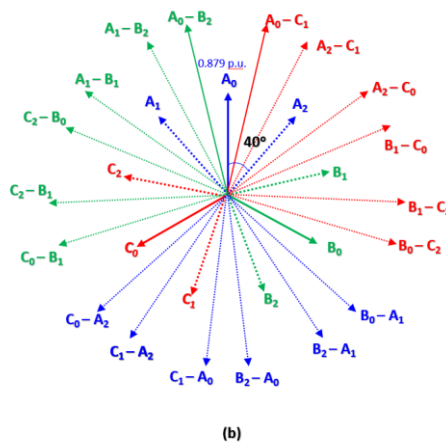
$$U_{out(LN)} = \frac{\sin 160^\circ}{\sin 10^\circ} U_{in(LN)} = 1.97 U_{in(LN)}. \quad (14)$$

The  $U_{dc}$  is the DC output voltage and could be calculated by (15) and (16) [18]:

$$U_{dc} = 0.995 U_{out(LL)}, \quad (15)$$



(a)



(b)

Fig. 3. Symmetric T-Delta: a) Connection Diagram; b) Conducting sequence.

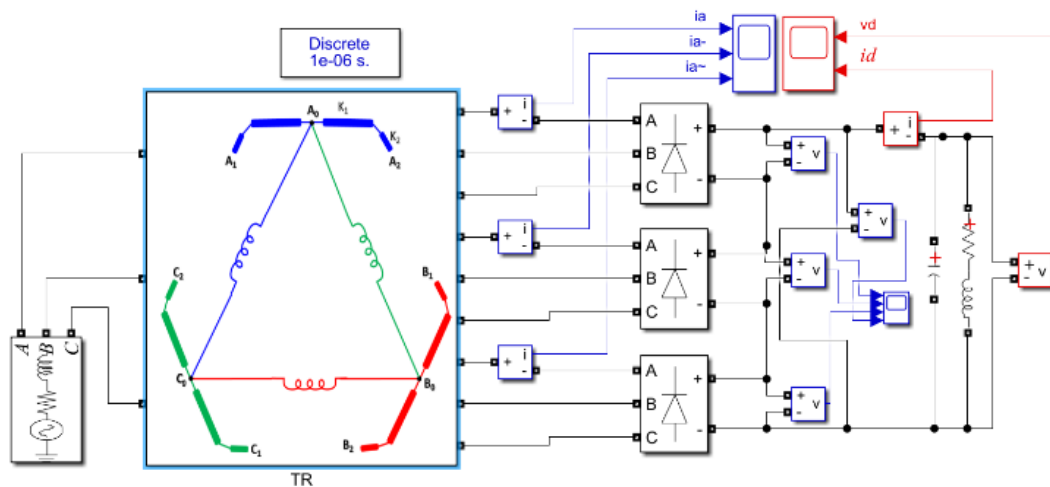


Fig. 4. MATLAB simulation of the symmetric T-Delta differential.

Using the same parameters, the total power capacity of the symmetric 18-PSAT T-Delta differential autotransformer equals 73 % of the load power.

$$U_{dc} = 1.73 \times 0.995 \times 1.97 U_{in(LN)} = 3.39 U_{in(LN)}. \quad (16)$$

Assuming  $K_1 = 0.35$  and  $K_2 = 0.48$ ,  $I_{in}$  input current calculated by (17) [20]

$$I_{in} = \sqrt{\frac{\left(\frac{1}{K_1}\right)^2 + 2\left(\frac{1}{K_2}\right)^2}{\frac{1}{K_1 K_2}}} \times \frac{\sqrt{2}}{3} I_{dc}. \quad (17)$$

Similarly, the power capacity of an autotransformer can be determined by adding the volt-amp ratings of all the windings and then dividing that total by two. After that, inserting in (16) and (17) obtain (18)

$$C_T = \frac{\sqrt{3} K_1 K_2}{0.78} \left( \frac{2K_1 + 2K_2 + \sqrt{K_1^2 + 2K_2^2}}{2K_1 K_2} \right) U_{dc} I_{dc} = 0.73 U_{dc} I_{dc}. \quad (18)$$

Figure 4 shows the MATLAB simulation of the second proposal symmetric 18-PSAT differential T-Delta.

### Symmetric 18-PSAT Delta Differential

The Delta differential configuration divides the input voltage into three identical sets (each set is three phase), and

between each set 40 degrees. Fig. 5(a) shows the connection diagram of the input terminal (power supply) and the output side (diode bridge). By sharing current with the other two diodes at a rate of 20 % each, each diode can carry 40 % of the total current. The conducting sequence of the diode current in the symmetric 18-PSAT Delta differential is shown in Fig. 5(b).

In the symmetric 18-PSAT Delta differential, the  $U_{out(LN)}$  is calculated as in (19) [19]

$$U_{out(LN)} = \frac{\sin 40^\circ}{\sin 120^\circ \sin 70^\circ} U_{in(LN)} = 1.66 U_{in(LN)}. \quad (19)$$

The  $U_{dc}$  is the DC output voltage and could be calculated by (20) and (21) [20]:

$$U_{dc} = 1.6 U_{out(LL)}, \quad (20)$$

$$U_{dc} = 1.73 \times 1.6 \times 1.66 U_{in(LN)} = 4.59 U_{in(LN)}. \quad (21)$$

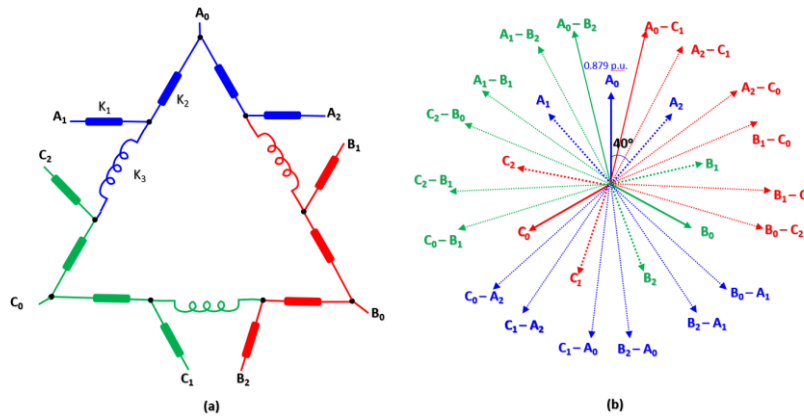


Fig. 5. (a) Connection diagram; (b) Conducting sequence of the diode current.

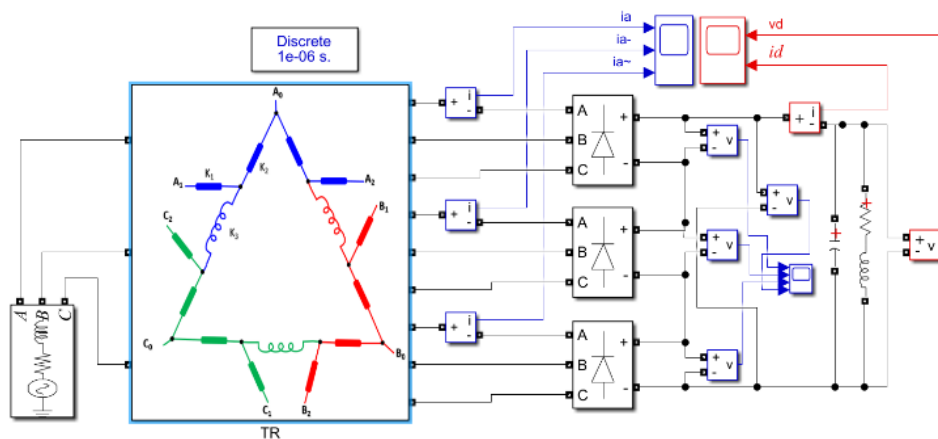


Fig. 6. MATLAB simulation of the symmetric Delta differential.

Using same parameters, the total power capacity of the symmetric 18-PSAT T-Delta differential autotransformer equals 85 % of the load power.

### C. Asymmetric 18-PSAT Delta Differential

In the symmetric fork, T-Delta, and Delta the total power flows through each bridge. But in the asymmetric Delta method, can be adjusted, so 2/3 of the total power flows through each bridge and the rest 1/3 flows through the primary of the autotransformer, leading to lower power losses and higher power capacity. The asymmetric Delta reduces the

Assuming  $K_1 = 0.35$  and  $K_2 = 0.48$ , the  $I_{in}$  input current is calculated by (22) [20]

$$I_{in} = \frac{\sqrt{2}}{3} I_{dc} \sqrt{2(K_1 + K_2)^2 + 6K_1^2 + 6K_2^2} = 0.88 I_{dc}. \quad (22)$$

A regular 6-pulse converter has a  $U_{dc}$  that is 18 % lower than the standard design. Using the same method, it should be possible to locate the remaining branch currents. Similarly, the power capacity of an autotransformer may be determined by (23) and (24):

$$C_T = 6K_1 U_{K_1} I_{K_1} + 6K_2 U_{K_2} I_{K_2} + 3K_3 U_{K_3} I_{K_3}, \quad (23)$$

$$\text{Total power capacity} = 0.85 U_{dc} I_{dc}. \quad (24)$$

Figure 6 shows the MATLAB simulation of the symmetric 18-PSAT Delta differential.

input voltage by 77 % and divides it into three identical sets (each set is three phase), and between each set 37 degrees. As a result, the DC voltage at output equals only 0.75 of line voltage, which is only 20 % more than in a standard design. Figure 7(a) shows the connection diagram of the input terminal (power supply) and the output side (diode bridge). Figure 7(b) depicts the conducting sequence of the diode current of the design.

In asymmetric 18-PSAT Delta differential, the  $U_{out(LN)}$  is calculated as in (25) [20]

$$U_{out(LN)} = \frac{\sin 120^\circ}{\sqrt{2} \sin 20^\circ \sin 80^\circ} U_{in(LN)} = 1.81 U_{in(LN)}. \quad (25)$$

The  $U_{dc}$  is the DC output voltage and could be calculated by (26) and (27) [20]:

$$U_{dc} = 1.45 U_{out(LL)}, \quad (26)$$

$$U_{dc} = 1.73 \times 1.45 \times 1.81 U_{in(LN)} = 4.54 U_{in(LN)}. \quad (27)$$

Assuming  $K_1 = 0.35$  and  $K_2 = 0.48$ , the  $I_{in}$  input current is calculated by (28) [20]

$$I_{in} = \frac{1}{3} I_{dc} \sqrt{2(K_1 + K_2)^2 + 6K_1^2 + 6K_2^2} = 0.62 I_{dc}. \quad (28)$$

Similarly, the power capacity of an autotransformer may be determined by (29) and (30):

$$C_T = 6K_1 U_{K_1} I_{K_1} + 6K_2 U_{K_2} I_{K_2} + 3K_3 U_{K_3} I_{K_3}, \quad (29)$$

$$\text{Total power capacity} = 0.80 U_{dc} I_{dc}. \quad (30)$$

Figure 8 shows the MATLAB simulation of the asymmetric 18-PSAT Delta differential.

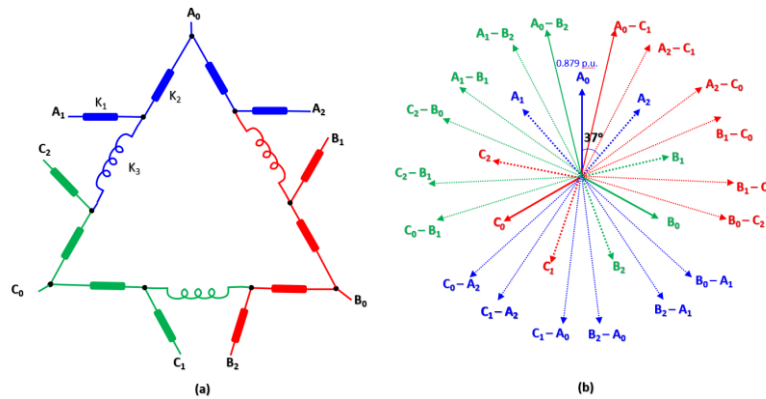


Fig. 7. (a) Connection diagram; b) Conducting sequence of the diode current.

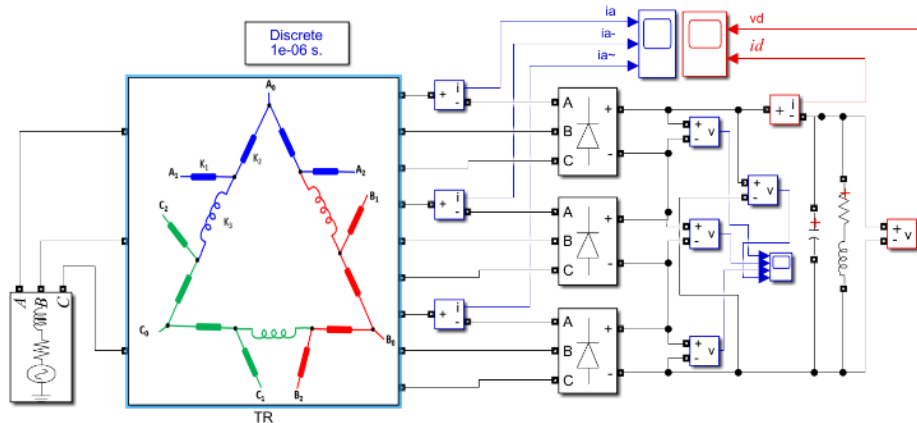


Fig. 8. MATLAB simulation of the asymmetric Delta differential.

Using the *same* parameters, the total power capacity of the symmetric 18-PSAT T-Delta differential autotransformer equals 80 % of the load power.

### III. RESULTS

The simulation results of the four topologies of 18-PSAT are discussed. Each topology was modelled using the MATLAB Simulink environment. The ideal current density adjusting equals ( $J_0 = 270\text{A}/\text{cm}^2$ ), the transformer windings turn were determined as  $K_1 = 0.35$ ,  $K_2 = 0.48$ ,  $K_3 = 0.15$ ,  $U_{in(LL)} = 380\text{V}$ ,  $R = 100\ \Omega$  and the  $V/\text{turn}$  ratio equals one. The duration of commutation for currents flowing through diodes is negligible in the virtual world. The input line current shows an 18-pulse rectification cycle during a single cycle. Noise and a longer commutation time both have a negative impact on the load characteristics. Using the input line current of the simulation, the THD of each proposed topology was calculated. Table I presents the findings of these odd harmonic measurements for each topology with the

limitations of the comparison harmonics of IEEE 519.

TABLE I. LINE CURRENT HARMONICS FOR PROPOSED DESIGNS.

Harmonic No.	IEEE Limits	Symm etric Fork	Symm etric T-Delta	Symm etric Delta	Asymmet ric Delta
3	2	0	0	0	0
5	2	0.1	0.1	0.1	0.1
7	2	0.3	0.2	0.1	0.1
9	1.1	0	0.2	0	0
11	3	0.2	0	0.1	0.1
13	3	0.3	0.1	0.1	0.1
15	3	0	0.1	0	0.2
17	4	1.4	1.3	1.2	1.3
19	4	1.6	1.6	1.3	1.3
THD	-	3.9	3.6	2.9	3.2

Simulation results, including transformer current output and rectifier current output, for the symmetric 18-PSAT fork differential, the symmetric 18-PSAT T-Delta differential, the symmetric 18-PSAT Delta differential, and the asymmetric 18-PSAT Delta differential are shown in Figs. 9–12,

respectively.

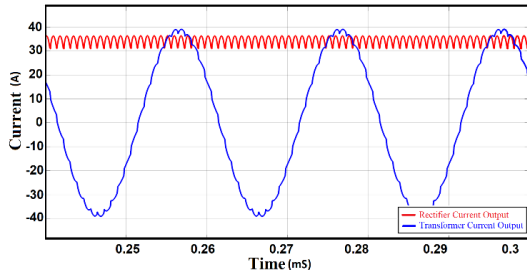


Fig. 9. MATLAB simulation results of symmetric fork differential.

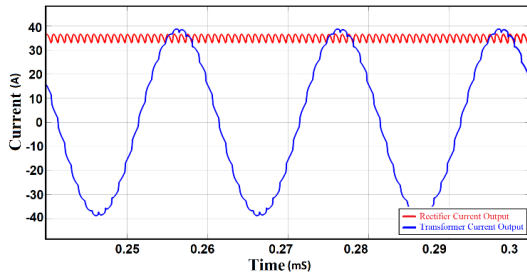


Fig. 10. MATLAB simulation results of the symmetric T-Delta differential.

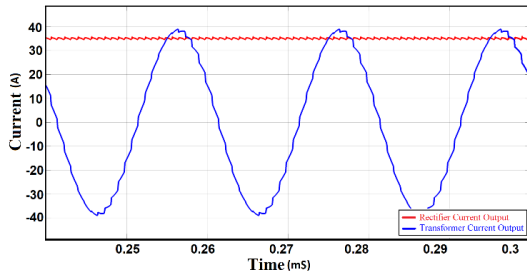


Fig. 11. MATLAB simulation results of symmetric Delta differential.

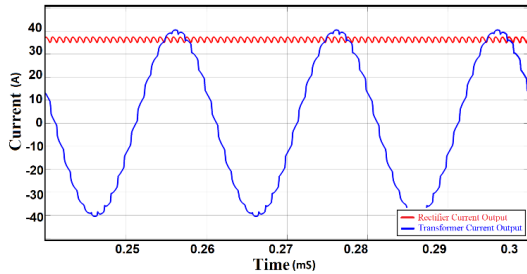


Fig. 12. MATLAB simulation results of asymmetric Delta differential.

#### IV. DISCUSSION

The simulation results of the symmetric 18-PSAT fork differential have smooth steps in the input line current. Ripples in the load characteristics are less than in the standard design, where the THD is equal to 3.9 %, which is well within the allowable range as defined by the IEEE guidelines for this setup. The simulation results of the symmetric 18-PSAT T-Delta differential have more smooth steps in the input line current than the fork differential. Ripples in the load characteristics are less than the fork differential, where the THD equals 3.6 %. The simulation results of the symmetric 18-PSAT Delta differential have more smooth steps in the input line current than the T-Delta differential. Ripples in the load characteristics are less than the T-Delta differential, where the THD equals 2.9 %. The simulation results of the asymmetric 18-PSAT Delta differential have more smooth steps in the input line current than the T-Delta differential but fewer smooth steps than the symmetric Delta differential.

Ripples in the load characteristics are less than the T-Delta differential, but more than the symmetric Delta differential. The THD equals 3.2 %. As a result, from simulation and mathematical discussion, the symmetric 18-PSAT Delta differential is simplicity, efficiency, and dependability between the configurations. According to design parameters found in the study, a symmetric 18-PSAT Delta differential was manufactured, and experimental results of transformer current output and rectifier current output are shown in Fig. 13.

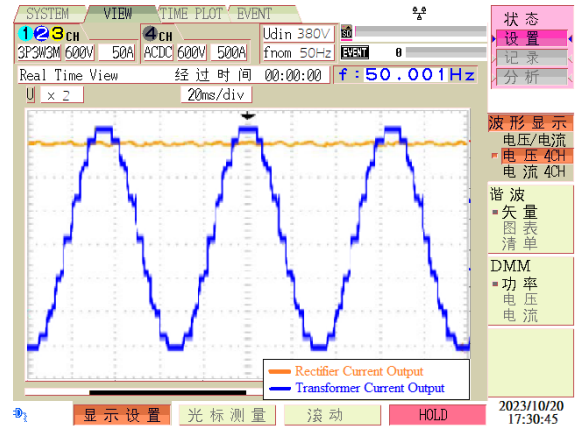


Fig. 13. Experimental results of the symmetric Delta differential design.

#### V. CONCLUSIONS

Implementing an autotransformer without additional components, such as an IPT or ZSBT, makes the system simpler and more efficient. Harmonic cancelation using an autotransformer is a method to eliminate the no characteristic low-order current harmonics. The symmetric 18-PSAT Delta differential proposal scheme is the most acceptable for use in systems because it has the miniature weight, size, and total harmonic distortion values. Although all schemes give harmonic levels within the IEEE 519 limitations. The proposed 18-PSAT advantages are that it does not need active switching devices since it is entirely passive. The suggested design of the symmetric 18-PSAT Delta differential satisfies industrial applications without needing an additional filter due to its low kVA rating and THD below IEEE 519 restrictions. The experimental results of the symmetric Delta differential design confirm and support the simulation results. The present study emphasises the dependability of circuits, the actual analysis of design, and the effects of open/short circuit defects on the effectiveness of PSAT.

#### VI. FUTURE WORK

This study is part of the doctoral thesis under “Medium Voltage Motor Drive Cascade Connected Multi-Level Type”. The Symmetric Delta differential design will be studied and analysed after connecting it with the multi-level cascade motor drive under no load and load status.

#### CONFLICTS OF INTEREST

The authors declare that they have no conflicts of interest.

#### REFERENCES

- [1] R. Abdollahi, G. B. Gharehpetian, F. Mohammadi, and S. Prakash P., “Multi-pulse rectifier based on an optimal Pulse Doubling Technique”, *Energies*, vol. 15, no. 15, p. 5567, 2022. DOI: 10.3390/en15155567.

- [2] Ö. F. Farsakoğlu, N. Aksoy, H. Y. Hasirci, and A. Alahmad, "Design and application of solar dish-gamma type stirling system", in *Proc. of 2018 5th International Conference on Electrical and Electronic Engineering (ICEEE)*, 2018, pp. 242–246. DOI: 10.1109/ICEEE2.2018.8391339.
- [3] R. Abdollahi, G. B. Gharehpetian, A. Anvari-Moghaddam, and F. Blaabjerg, "Pulse tripling circuit and twelve pulse rectifier combination for sinusoidal input current", *IEEE Access*, vol. 9, pp. 103588–103599, 2021. DOI: 10.1109/ACCESS.2021.3098620.
- [4] K.-P. Huang, H.-I. Hsieh, and R.-J. Wai, "Phase-shifted full-bridge converter for a half-current-multiplier rectifier using an autotransformer-based filter", *IEEE Transactions on Transportation Electrification*, vol. 6, no. 1, pp. 199–212, 2020. DOI: 10.1109/TTE.2020.2971344.
- [5] S. Khan, X. Zhang, M. Saad, H. Ali, B. M. Khan, and H. Zaman, "Comparative analysis of 18-pulse autotransformer rectifier unit topologies with intrinsic harmonic current cancellation", *Energies*, vol. 11, no. 6, p. 1347, 2018. DOI: 10.3390/en11061347.
- [6] A. Alahmad and F. Kaçar, "Simulation of induction motor driving by bridge inverter at 120°, 150°, and 180° operation", in *Proc. of 2021 8th International Conference on Electrical and Electronics Engineering (ICEEE)*, 2021, pp. 121–125. DOI: 10.1109/ICEEE52452.2021.9415930.
- [7] X. Yan, F. Qin, J. Jia, Z. Zhang, X. Li, and Y. Sun, "Virtual synchronous motor based-control of Vienna rectifier", *Energy Reports*, vol. 6, pp. 953–963, 2020. DOI: 10.1016/j.egy.2020.11.098.
- [8] C.-m. Young, M.-h. Chen, C.-h. Lai, and D.-C. Shih, "A novel control for active interphase transformer using in a 24-pulse converter", in *Proc. of The 2010 International Power Electronics Conference - ECCE ASIA*, 2010, pp. 2086–2091. DOI: 10.1109/IPEC.2010.5543617.
- [9] A. Alahmad, F. Kaçar, Ö. F. Farsakoğlu, and C. P. Uzunoğlu, "Medium-voltage drives (MVD) - Pulse width modulation (PWM) techniques", in *Proc. of 2023 Second International Conference on Electronics and Renewable Systems (ICEARS)*, 2023, pp. 91–94. DOI: 10.1109/ICEARS56392.2023.10084995.
- [10] R. Abdollahi, "Multi-Phase Shifting Autotransformer based rectifier", *IEEE Open Journal of the Industrial Electronics Society*, vol. 1, pp. 38–45, 2020. DOI: 10.1109/OJIES.2020.2984715.
- [11] A. Alahmad, "Using medium voltage variable frequency drives instead of medium voltage switchgear in a pump system", *Indian Journal of Signal Processing (IJSP)*, vol. 3, no. 1, pp. 1–5, 2023. DOI: 10.54105/ijsp.B1014.023123.
- [12] X. Chen, T. Chen, and Y. Wang, "Investigation on design of novel step-up 18-pulse auto-transformer rectifier", *IEEE Access*, vol. 9, pp. 110639–110647, 2021. DOI: 10.1109/ACCESS.2021.3103584.
- [13] T. Al-Mhana, V. Pickert, D. J. Atkinson, and B. Zahawi, "Forced commutated controlled series capacitor rectifier for more electric aircraft", *IEEE Transactions on Power Electronics*, vol. 34, no. 1, pp. 225–235, 2019. DOI: 10.1109/TPEL.2018.2816305.
- [14] J. Chen, C. Wang, and J. Chen, "Investigation on the selection of electric power system architecture for future more electric aircraft", *IEEE Transactions on Transportation Electrification*, vol. 4, no. 2, pp. 563–576, 2018. DOI: 10.1109/TTE.2018.2792332.
- [15] S. Karmakar and B. Singh, "96-pulse VSC based large-scale grid interfaced solar PV plant with distributed MPPT and DC-coupled battery energy storage", in *Proc. of 2022 IEEE Global Conference on Computing, Power and Communication Technologies (GlobConPT)*, 2022, pp. 1–6. DOI: 10.1109/GlobConPT57482.2022.9938160.
- [16] F. Meng, X. Xu, and L. Gao, "A simple harmonic reduction method in multipulse rectifier using passive devices", *IEEE Transactions on Industrial Informatics*, vol. 13, no. 5, pp. 2680–2692, 2017. DOI: 10.1109/TII.2017.2723602.
- [17] R. Abdollahi and G. B. Gharehpetian, "A 20-pulse autotransformer rectifier unit for more electric aircrafts", *IEEE Journal of Emerging and Selected Topics in Power Electronics*, vol. 9, no. 3, pp. 2992–2999, 2021. DOI: 10.1109/JESTPE.2020.2990670.
- [18] R. Abdollahi, G. B. Gharehpetian, A. Anvari-Moghaddam, and F. Blaabjerg, "A 40-pulse autotransformer rectifier based on new pulse multiplication circuit for aviation application", *IEEE Transactions on Industrial Electronics*, vol. 70, no. 11, pp. 10822–10832, 2023. DOI: 10.1109/TIE.2022.3227229.
- [19] R. Abdollahi, G. B. Gharehpetian, and M. Davari, "A novel more electric aircraft power system rectifier based on a low-rating autotransformer", *IEEE Transactions on Transportation Electrification*, vol. 8, no. 1, pp. 649–659, 2022. DOI: 10.1109/TTE.2021.3104576.
- [20] C. P. Uzunoğlu, A. Alahmad, and F. Kaçar, "Medium-voltage drives (MVD) - Performance analysis of seven-level cascaded H-bridge multilevel driver", *WSEAS Transactions on Electronics*, vol. 14, pp. 57–64, 2023. DOI: 10.37394/232017.2023.14.7.



This article is an open access article distributed under the terms and conditions of the Creative Commons Attribution 4.0 (CC BY 4.0) license (<http://creativecommons.org/licenses/by/4.0/>).